Crystal structure and dielectric properties of the $[(CH_3)_2NH_2]_3Sb_{2(1-x)}Bi_{2x}Cl_9$ (DMACAB) mixed crystals

2001 J. Phys.: Condens. Matter 13 8831

(http://iopscience.iop.org/0953-8984/13/39/310)

INSTITUTE OF PHYSICS PUBLISHING JOURNAL OF PHYSICS: CONDENSED MATTER

J. Phys.: Condens. Matter **13** (2001) 8831–8852 PII: S0953-8984(01)22898-7

Crystal structure and dielectric properties of the $[(CH_3)_2NH_2]_3Sb_{2(1-x)}Bi_{2x}Cl_9$ (DMACAB) mixed crystals

M Wojtaś[1], G Bator[1], R Jakubas[1] and J Zaleski[2]

[1] Faculty of Chemistry, University of Wroclaw, Joliot-Curie 14, 50-383 Wroclaw, Poland
[2] Institute of Chemistry, University of Opole, Oleska 48, 45-951 Opole, Poland

Received 15 March 2001, in final form 16 July 2001
Published 13 September 2001
Online at stacks.iop.org/JPhysCM/13/8831

Abstract

Phase transitions in $[(CH_3)_2NH_2]_3Sb_{2(1-x)}Bi_{2x}Cl_9$ (DMACAB) mixed salts in the composition range $0 \leqslant x \leqslant 0.41$ have been investigated by the pyroelectric method and dielectric measurements over the frequency range from 75 kHz to 900 MHz. The phase situation is additionally confirmed by the differential scanning calorimetry (DSC) and dilatometric techniques. A transition from the paraelectric (PE) to the ferroelectric (FE) phase is observed for crystals with $0 \leqslant x \leqslant 0.14$. Pyroelectric measurements support the presence of polar phases. The dynamic dielectric behaviour of ferroelectric systems is found to be determined by the existence of two independent relaxators. The low-frequency relaxator reveals a critical slowing down of its dynamics in the close vicinity of the PE $\rightarrow$ FE transition. For compositions in the range $0.17 \leqslant x \leqslant 0.41$ a new sequence of phase transitions appears without any polar phases being present. The disappearance of ferroelectric properties is related to the fundamental changes in the crystal structure of the mixed compounds. The characteristic feature of the ferroelectric mixed crystals ($0.0 \leqslant x \leqslant 0.14$) is the presence of polyanionic $(M_2Cl_9^{3-})_n$ (M = Sb, Bi) layers, whereas non-ferroelectric ones are characterized by a different anionic sublattice composed of polyanionic one-dimensional double chains.

1. Introduction

The physical properties of the alkylammonium halogenoantimonates(III) and bismuthates(III) with general formula $R_aM_bX_{(3b+a)}$ (R = organic cation; M = Sb, Bi; X = Cl, Br, I) have attracted considerable attention in recent years [1–4]. Several crystals belonging to this family reveal ferroelectric properties. Their dielectric parameters are of interest for practical applications. The polar properties are found only for crystals of the $R_5M_2X_{11}$ and $R_3M_2X_9$ stoichiometries. All salts of the $R_5M_2X_{11}$ stoichiometry known up to now exhibit ferroelectric properties. They contain isolated bioctahedral units $Bi_2X_{11}^{5-}$ in their crystal lattice [5,6]. On the

other hand the $R_3M_2X_9$ family possesses four different anionic sub-units. The MX_6 octahedra are connected with each other by corners, edges or faces forming: infinite one-dimensional chains (type a) [7], two-dimensional layers (b) [8], isolated bioctahedral units (c) [9] and four octahedral units (d) [10]. The ferroic (ferroelectric) properties are found only for the b-type compounds. The $[(CH_3)_2NH_2]_3Sb_2Cl_9$ (DMACA) crystal, which belongs to this subgroup of crystals, reveals for instance the following phase situation [11]:

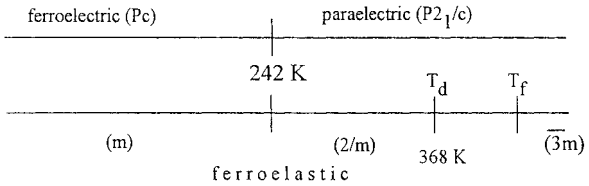

where T_f indicates the ferroelastic phase transition that would be expected if the crystal did not decompose at T_d.

In the paraelectric phase, two crystallographically non-equivalent dimethylammonium (DMA) cations are found in the unit cell: one disordered cation is located about at the centre of symmetry inside the polyanionic cavities; the other one is located at the general position between the polyanionic layers [12]. The mechanism of the PE $\rightarrow$ FE phase transition is attributed to ordering of the DMA cations located in the polyanionic cavities. The dynamical reorientations of these cations between two positions are frozen at T_c, which results in the appearance of spontaneous polarization in the ac-plane. Dielectric dispersion measurements reveal a critical slowing down of the relaxation frequency in the paraelectric phase [13]. Raman single-crystal studies show a continuous change in the frequencies of Raman bands at 242 K with no soft-mode behaviour [14, 15].

The pure antimony analogue, DMACA, is a classical example of a system with a pure order–disorder mechanism of the PE $\rightarrow$ FE phase transition. Its dielectric parameters are interesting not only from the point of view of fundamental research, but may also be important from the point of view of technical applications. The goal of the present investigation is the determination of the influence of metal-atom replacement (Sb $\rightarrow$ Bi) on the structure and dielectric characteristics of the mixed $[(CH_3)_2NH_2]_3Sb_{2(1-x)}Bi_{2x}Cl_9$ (DMACAB) crystals. The results of studies on the pure bismuth analogue $[(CH_3)_2NH_2]_3Bi_2Cl_9$ (DMACB) are presented for the first time. In the present paper, special attention is paid to the dynamics of the dielectric properties of the title crystals. Hence through these investigations we can gain a microscopic understanding of the ferroelectric behaviour of the halogenoantimonate(III) and bismuthate(III) crystals.

2. Experimental details

Mixed crystals of $[(CH_3)_2NH_2]_3Sb_{2(1-x)}Bi_{2x}Cl_9$ were obtained by slow evaporation of an aqueous solution containing $(CH_3)_2NH$, $SbCl_3$ and $BiCl_3$ with an excess of HCl. The ratio of Sb to Bi was estimated by elemental analysis. Mixed crystals with the following Bi contents were obtained and studied: $x = 0.05, 0.09, 0.14, 0.17, 0.30, 0.36$ and 0.41. We did not succeed in preparing DMACAB crystals with x greater than 0.41, although we were able to grow the pure bismuth analogue: $[(CH_3)_2NH_2]_3Bi_2Cl_9$ (DMACB) crystal.

The complex electric permittivity $\varepsilon^* = \varepsilon' - i\varepsilon''$ was measured by an HP 4285A Precision LCR Meter in the frequency range between 75 kHz and 20 MHz and by an HP 4191A Impedance Analyser in the frequency range between 30 MHz and 900 MHz in the temperature range from

140 to 300 K. The dimensions of the sample studied were of the order of $5 \times 3 \times 1$ mm^3. The overall error was less than 5% and 10% for the real and imaginary parts of the complex electric permittivity, respectively.

The spontaneous polarization was measured between 170 and 260 K by a charge-integration technique using a Keithley 617 Programmable Electrometer. The temperature was stabilized by the temperature controller Instec STC200.

Differential scanning calorimetry (DSC) measurements were carried out using a Perkin-Elmer DSC-7 in the temperature range 100–400 K.

Dilatometric measurements were performed using a thermomechanical analyser, Perkin-Elmer TMA-7, in the temperature range 140–300 K. The dimensions of the sample were of the order of $5 \times 3 \times 1$ mm^3.

Data for the structure determination for DMACAB with $x = 0.14$ and $x = 0.38$ were collected at room temperature on a KM-4 KUMA diffractometer with Mo Kα radiation. The lattice parameters were refined from setting angles of 24 reflections in the $20^\circ < 2\theta < 25^\circ$ range. The reflections were collected using the ω–θ scan technique; scan speed: 0.03–0.15 s^{-1}; scan width: 1°. Two control reflections measured after intervals of 50 reflections showed negligible intensity variation. Lorentz-polarization and semi-empirical absorption corrections were applied. The SHELXS/SHELXL [16] programs were used for structure calculations. The crystal data and measurement parameters are presented in table 1.

Table 1. Crystal data and structure refinement for $[NH_2(CH_3)_2]_3Sb2_{1-x}Bi_{2x}Cl_9$, $x = 0.14$, 0.38.

Empirical formula	$[NH_2(CH_3)_2]_3Sb2_{1-x}Bi_{2x}Cl_9$	
x	0.14	0.38
Formula weight	725.3	766.3
Temperature	293(2) K	
Wavelength	0.71073 Å	
Crystal system, space group	Monoclinic $P2_1/c$	Orthorhombic $Pnma$
Unit-cell dimensions	$a = 9.688(2)$ Å $b = 9.009(2)$ Å $c = 14.066(3)$ Å $\beta = 95.49(3)^\circ$	$a = 21.287(4)$ Å $b = 8.143(2)$ Å $c = 14.130(3)$ Å
Volume	1222.0(5) Å^3	2449.3(9) Å^3
Z, calculated density	2, 1.971 g cm^{-3}	4, 2.078 g cm^{-3}
Density measured	1.95(1)	2.09(1)
Absorption coefficient	4.898 mm^{-1}	7.736 mm^{-1}
$F(000)$	690	1440
Theta range for data collection	3 to 25°	
Reflections collected/unique	2308/2172	1577/1577
Refinement method	Full-matrix least-squares on F^2	
Data/restraints/parameters	2172/61/117	1577/69/132
Goodness-of-fit on F^2	1.057	1.004
Final R-indices ($I > 2\sigma(I)$)	$R_1 = 0.0300$, $wR_2 = 0.0806$	$R_1 = 0.0394$ $wR_2 = 0.1060$
R-indices (all data)	$R_1 = 0.0412$ $wR_2 = 0.0852$	$R_1 = 0.1315$ $wR_2 = 0.1327$
Largest diffraction peak and hole	0.438/−0.472 e Å^{-3}	0.518/−0.502 e Å^{-3}

The structure was solved by the Patterson method, which revealed the positions of the antimony, bismuth and chlorine atoms. Subsequent difference Fourier synthesis revealed the positions of the carbon and nitrogen atoms. The hydrogen atoms were introduced from

geometric criteria and were not refined. The atomic coordinates and equivalent isotropic displacement parameters for DMACAB with $x = 0.14$ and 0.38 are presented in table 2. The inter-atomic distances and angles are given in tables 3 and 4.

Table 2. Atomic coordinates ($\times 10^4$) and equivalent isotropic displacement parameters (10^3 Å^2) for $[NH_2(CH_3)_2]_3Sb2_{1-x}Bi_{2x}Cl_9$, $x = 0.14$, 0.38. U_{eq} is defined as one third of the trace of the orthogonalized U_{ij}-tensor.

	x	y	z	U_{eq}
$x = 0.14$				
Sb(1)	3395(1)	396(1)	1640(1)	48(1)
Bi(1)	3384(3)	361(4)	1633(3)	45(1)
Cl(1)	2089(2)	2211(2)	664(1)	83(1)
Cl(2)	2091(2)	841(2)	3033(1)	77(1)
Cl(3)	1588(2)	−1477(2)	1065(1)	82(1)
Cl(4)	4822(2)	−2227(2)	2765(1)	87(1)
Cl(5)	5000	0	0	127(1)
N(11)	1686(17)	−679(14)	−1351(9)	178(6)
N(12)	1560(5)	−1210(3)	−2130(2)	123(11)
C(1)	1250(9)	−1999(11)	−1440(6)	109(3)
C(2)	1906(12)	254(11)	−2136(11)	163(5)
N(2)	4623(15)	−5655(16)	−42(12)	106(4)
C(3)	4121(10)	−4274(10)	332(7)	107(3)
$x = 0.38$				
Sb(1)	1553(1)	2500	802(2)	101(1)
Sb(2)	−155(1)	−2500	2530(1)	95(1)
Bi(1)	1565(1)	2500	928(2)	111(1)
Bi(2)	79(1)	−2500	2519(2)	100(1)
Cl(1)	2189(2)	2500	2353(4)	219(3)
Cl(2)	2216(2)	282(7)	197(3)	231(2)
Cl(3)	907(2)	2500	−944(3)	182(2)
Cl(4)	778(2)	31(6)	1746(3)	214(2)
Cl(5)	596(4)	−2500	3998(4)	226(3)
Cl(6)	−707(2)	−363(6)	3240(3)	207(2)
N(1)	2425(4)	2500	−2127(8)	490(3)
C(1)	2922(5)	2500	−2374(19)	300(17)
C(2)	2193(12)	2500	−2840(12)	640(5)
N(2)	−811(4)	2500	1206(9)	500(3)
C(3)	−1328(6)	2500	1370(2)	410(3)
C(4)	−571(10)	2500	499(10)	258(15)
N(3)	872(4)	1730(2)	4203(15)	272(16)
C(5)	448(7)	2500	4056(16)	276(18)
C(6)	1346(7)	1650(3)	4559(17)	178(12)

3. Results

3.1. X-ray studies

DMACAB with the concentration $x = 0.14$ is isomorphous with the two pure antimony analogues $[(CH_3)_2NH_2]_3Sb_2Cl_9$ (DMACA) [17] and $[(CH_3)_2NH_2]_3Sb_2Br_9$ (DMABA) [18]. It crystallizes in the monoclinic $P2_1/c$ space group. The lattice parameters are almost equal to

Table 3. Selected bond lengths (Å) and angles (deg) for $[NH_2(CH_3)_2]_3Sb2_{1-x}Bi_{2x}Cl_9$, $x = 0.14$. (Symmetry transformations used to generate equivalent atoms: No 1: $-x+1, y+1/2, -z+1/2$; No 2: $-x+1, y-1/2, -z+1/2$; No 3: $-x+1, -y, -z$; No 4: $-x+1, -y-1, -z$.)

Sb(1)–Cl(1)	2.414(2)
Sb(1)–Cl(2)	2.462(2)
Sb(1)–Cl(3)	2.509(2)
Sb(1)–Cl(4)	3.095(2)
Sb(1)–Cl(4), No 1	2.827(2)
Sb(1)–Cl(5)	2.925(1)
Bi(1)–Cl(1)	2.426(4)
Bi(1)–Cl(2)	2.470(4)
Bi(1)–Cl(3)	2.479(4)
Bi(1)–Cl(4)	3.080(4)
Bi(1)–Cl(4), No 1	2.859(4)
Bi(1)–Cl(5)	2.919(4)
Cl(1)–Sb(1)–Cl(2)	93.50(7)
Cl(1)–Sb(1)–Cl(3)	87.73(7)
Cl(1)–Sb(1)–Cl(4)	172.77(7)
Cl(1)–Sb(1)–Cl(4), No 1	85.84(7)
Cl(1)–Sb(1)–Cl(5)	85.60(6)
Cl(2)–Sb(1)–Cl(3)	88.35(7)
Cl(2)–Sb(1)–Cl(4)	87.49(6)
Cl(2)–Sb(1)–Cl(4), No 1	89.23(7)
Cl(2)–Sb(1)–Cl(5)	177.41(6)
Cl(3)–Sb(1)–Cl(4)	85.14(7)
Cl(3)–Sb(1)–Cl(4), No 1	172.98(7)
Cl(3)–Sb(1)–Cl(5)	94.04(6)
Cl(4), No 1–Sb(1)–Cl(4)	101.34(4)
Cl(4), No 1–Sb(1)–Cl(5)	88.28(5)
Cl(5)–Sb(1)–Cl(4)	93.71(5)
Cl(1)–Bi(1)–Cl(2)	93.02(13)
Cl(1)–Bi(1)–Cl(3)	88.17(12)
Cl(1)–Bi(1)–Cl(4)	174.09(17)
Cl(1)–Bi(1)–Cl(4), No 1	84.91(13)
Cl(1)–Bi(1)–Cl(5)	85.52(12)
Cl(2)–Bi(1)–Cl(3)	88.86(14)
Cl(2)–Bi(1)–Cl(4)	87.70(12)
Cl(2)–Bi(1)–Cl(4), No 1	88.34(12)
Cl(2)–Bi(1)–Cl(5)	175.96(17)
Cl(3)–Bi(1)–Cl(4)	85.98(13)
Cl(3)–Bi(1)–Cl(4), No 1	172.39(15)
Cl(3)–Bi(1)–Cl(5)	94.84(12)
Cl(4), No 1–Bi(1)–Cl(5)	87.79(12)
Cl(4), No 1–Bi(1)–Cl(4)	100.97(9)
Cl(5)–Bi(1)–Cl(4)	94.15(10)
Sb(1), No 2–Cl(4)–Sb(1)	163.75(7)
Sb(1)–Cl(5)–Sb(1), No 3	180.0
Bi(1)–Cl(5)–Bi(1), No 3	180.0
Bi(1), No 2–Cl(4)–Bi(1)	163.81(7)

those of DMACA crystal with only a slightly larger b-parameter (by 0.028 Å) and β-angle (by 0.08°). The anionic sublattice consists of two-dimensional polyanionic layers composed of the MCl_6^{3-} (M = Bi, Sb) deformed octahedra (figure 1). They are connected with each other

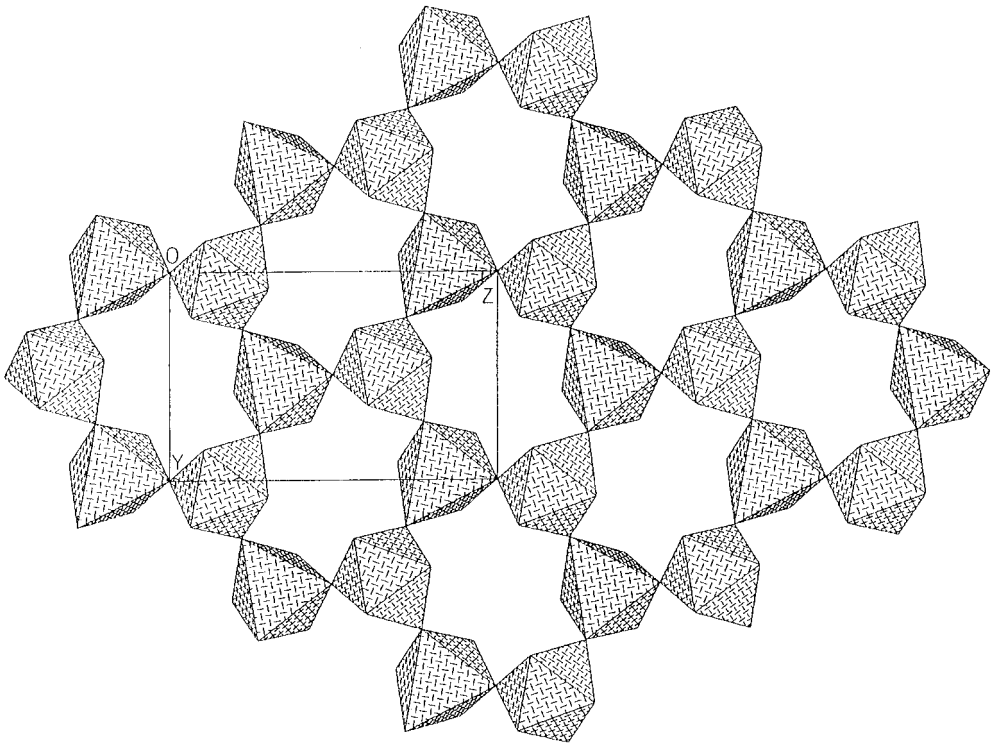

Figure 1. A two-dimensional layer of the anionic sublattice for mixed systems with $0 \leqslant x \leqslant 0.14$ as a polyhedral representation.

Table 4. Selected bond lengths (Å) and angles (deg) for $[NH_2(CH_3)_2]_3Sb_{2-x}Bi_{2x}Cl_9$, $x = 0.38$. (Symmetry transformations used to generate equivalent atoms: No 1: $-x, -y, -z$; No 2: $x, -y + 1/2, z$; No 3: $x, -y - 1/2, z$.)

Sb(1)–Cl(1)	2.577(6)
Sb(1)–Cl(2)	2.446(5)
Sb(1)–Cl(3)	2.824(6)
Sb(1)–Cl(4)	2.923(4)
Sb(2)–Cl(3), No 1	2.754(6)
Sb(2)–Cl(4)	3.069(4)
Sb(2)–Cl(5)	2.620(6)
Sb(2)–Cl(6)	2.328(4)
Bi(1)–Cl(1)	2.412(6)
Bi(1)–Cl(2)	2.499(5)
Bi(1)–Cl(3)	2.993(6)
Bi(1)–Cl(4)	2.861(4)
Bi(2)–Cl(3), No 1	3.059(6)
Bi(2)–Cl(4)	2.767(4)
Bi(2)–Cl(5)	2.363(6)
Bi(2)–Cl(6)	2.620(4)

by corners in such a way that three chlorine atoms of each octahedron are bridging and three are terminal. The terminal M–Cl bonds are shorter than the bridging ones. The terminal bonds involving antimonies are in the range 2.414–2.509 Å, whereas those involving the bismuth

Table 4. (Continued)

Cl(2)–Sb(1)–Cl(1)	89.6(2)
Cl(2)–Sb(1)–Cl(2), No 2	95.2(3)
Cl(2)–Sb(1)–Cl(3)	88.6(2)
Cl(2)–Sb(1)–Cl(4), No 2	173.2(2)
Cl(2), No 2–Sb(1)–Cl(4), No 2	88.7(2)
Cl(1)–Sb(1)–Cl(3)	177.4(2)
Cl(1)–Sb(1)–Cl(4), No 2	84.7(1)
Cl(3)–Sb(1)–Cl(4)	97.2(1)
Cl(4), No 2–Sb(1)–Cl(4)	86.9(2)
Cl(6), No 3–Sb(2)–Cl(6)	96.8(2)
Cl(6)–Sb(2)–Cl(5)	88.1(2)
Cl(6)–Sb(2)–Cl(3), No 1	93.3(1)
Cl(5)–Sb(2)–Cl(3), No 1	177.9(2)
Cl(6), No 3–Sb(2)–Cl(4)	169.9(2)
Cl(6)–Sb(2)–Cl(4)	88.9(2)
Cl(5)–Sb(2)–Cl(4)	83.7(2)
Cl(3), No 1–Sb(2)–Cl(4)	94.8(1)
Cl(4)–Sb(2)–Cl(4), No 3	84.4(2)
Cl(1)–Bi(1)–Cl(2)	92.3(2)
Cl(2)–Bi(1)–Cl(2), No 2	92.5(3)
Cl(2)–Bi(1)–Cl(4), No 2	177.8(2)
Cl(1)–Bi(1)–Cl(4)	89.2(2)
Cl(2)–Bi(1)–Cl(4)	89.1(2)
Cl(4), No 2–Bi(1)–Cl(4)	89.3(2)
Cl(1)–Bi(1)–Cl(3)	174.5(2)
Cl(2)–Bi(1)–Cl(3)	83.9(1)
Cl(4)–Bi(1)–Cl(3)	94.8(1)
Cl(5)–Bi(2)–Cl(6)	87.3(2)
Cl(6), No 3–Bi(2)–Cl(6)	83.2(2)
Cl(5)–Bi(2)–Cl(4)	95.6(2)
Cl(6), No 3–Bi(2)–Cl(4)	172.6(2)
Cl(6)–Bi(2)–Cl(4)	90.1(1)
Cl(4)–Bi(2)–Cl(4), No 3	96.3(2)
Cl(5)–Bi(2)–Cl(3), No 1	164.5(2)
Cl(6)–Bi(2)–Cl(3), No 1	81.1(1)
Cl(4)–Bi(2)–Cl(3), No 1	94.7(1)
Sb(1)–Cl(4)–Sb(2)	172.7(2)
Sb(2), No 1–Cl(3)–Sb(1)	173.6(2)
Bi(1)–Cl(3)–Bi(2), No 1	164.6(2)
Bi(2)–Cl(4)–Bi(1)	176.3(2)

atoms are in the range 2.426–2.479 Å. The bridging bonds are in the range 2.827–3.095 Å (Sb–Cl) and 2.859–3.080 Å (Bi–Cl). In this case, also, the deformation is slightly larger in the case of the antimony octahedra in comparison to the bismuth ones.

It should be noted that each short bond is opposite to a long one. The Sb–Cl bond lengths are almost the same as in the structure of the pure antimony salt, DMACA [12]. In the independent part of the unit cell there are two crystallographically independent dimethylammonium cations. One is located between the polyanionic layers, whereas the second one is located inside the polyanionic voids, formed by six MCl_6^{3-} octahedra (figure 2). Both types of cation are disordered, like in the case of pure DMACA crystal. The disorder is realized by splitting of the position of the nitrogen atom between two sites (figure 3). The nitrogen atom of the

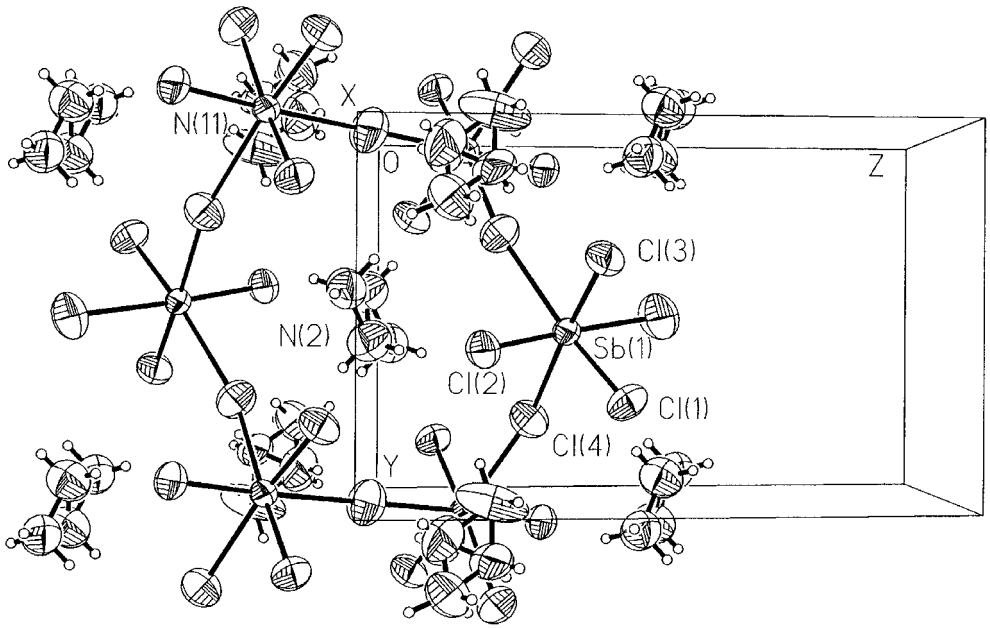

Figure 2. Projection of the crystal structure of DMACAB ($x = 0.14$) in the a-direction at 293 K.

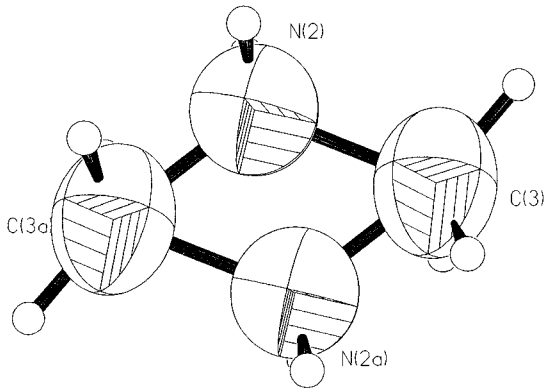

Figure 3. The disordered dimethylammonium cation N(2) in the DMACAB crystal ($x = 0.14$) at 293 K.

cation located inside the polyanionic cavity has half-occupancy, whereas that between the polyanionic layers has occupancies 0.80 and 0.20 for N(11) and N(12), respectively.

For Bi content above $x \geqslant 0.18$, the salts crystallize in the orthorhombic *Pnma* space group. The structure of DMACAB with $x = 0.38$ is isomorphous with the methylammonium antimonate(III) and bismuthate(III) analogues [7, 19]. The anionic sublattice of these salts is composed of one-dimensional $(M_2Cl_9^{3-})_n$ double chains (figure 4). There are three bridging and three terminal chlorine atoms in each octahedron. Each bridging bond is located opposite to a terminal one. The MX_6^{3-} octahedra are even more deformed than in the case of DMACAB with $x = 0.14$. The terminal Sb–Cl bonds are in the range 2.328–2.620 Å, whereas the bridging ones are in the range 2.754–3.069 Å. In the case of Bi–Cl bonds they are in the range 2.363–2.620 Å

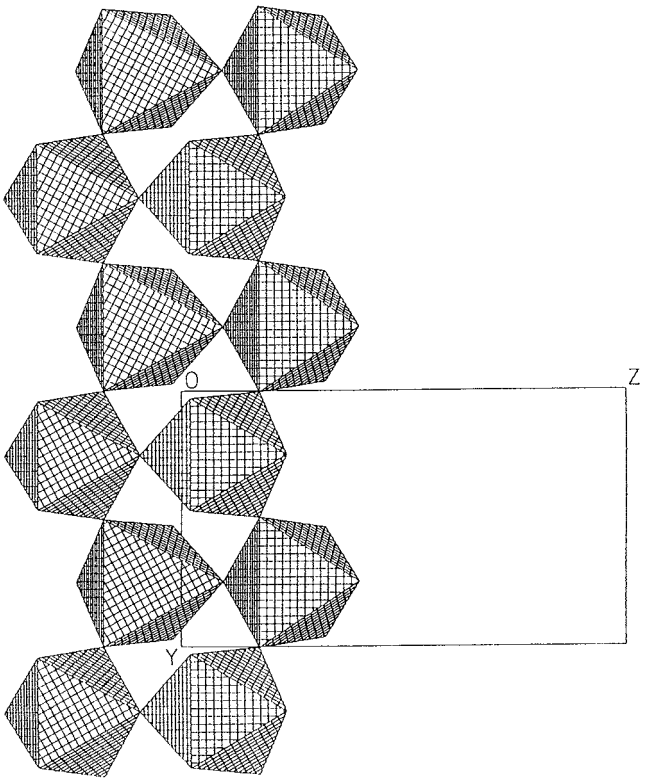

Figure 4. The one-dimensional double chain of the anionic sublattice for mixed systems with $0.17 \leqslant x \leqslant 0.41$ as a polyhedral representation.

for the terminal and 2.767–3.059 Å for the bridging ones. In both cases the M(2) octahedron is significantly more deformed than the M(1) one. The bond-length difference between the longest and shortest bonds for the Sb(1) octahedron is equal to 0.581 Å, whereas for Sb(2) it is equal to 0.696 Å. There are three crystallographically independent dimethylammonium cations in the crystal structure. The cations are characterized by very large thermal motions. A model of their disorder could not be determined.

3.2. DSC and dilatometric results

The DSC measurements show that there are two types of mixed DMACAB crystal characterized by different sequences of phase transitions. The first group with the Bi content ranging from 0 to 0.14 exhibits only one phase transition similarly to pure DMACA. The temperature of this phase transition strongly depends on the Bi content. The other group of these mixed crystals ($0.17 \leqslant x \leqslant 0.41$) reveals two phase transitions.

Figure 5 shows typical DSC runs on cooling and heating (at the rate of 10 K min^{-1}) for the DMACAB crystals with $x = 0$, 0.14, 0.17 and 0.41. The transition temperatures and corresponding heat effects are collected in table 5. The calorimetric measurements show that for $0 \leqslant x \leqslant 0.14$ we deal with one second-order phase transition and that the transition temperature decreases with increasing Bi content. On the other hand for crystals with $0.17 \leqslant x \leqslant 0.41$ two phase transitions of the first-order type are revealed. The low-

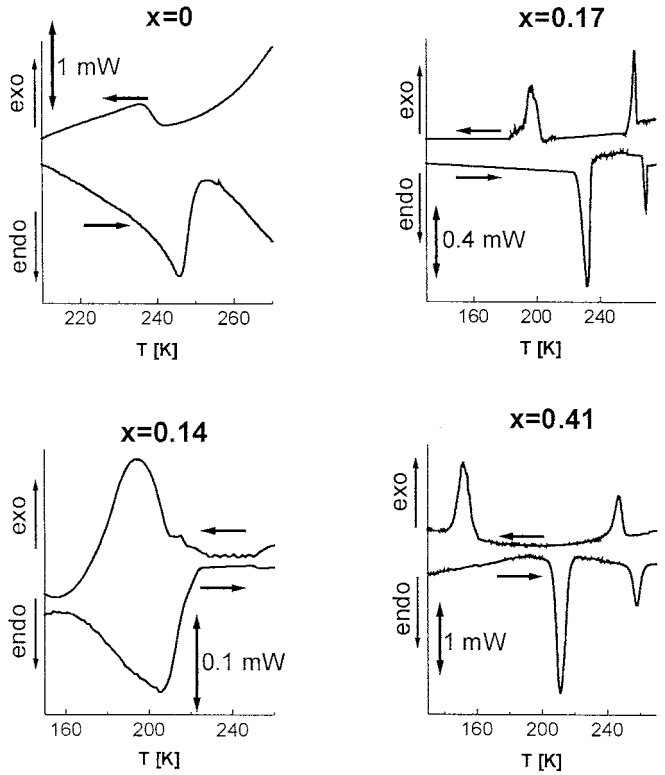

Figure 5. DSC curves of the DMACAB crystals with the Bi content $x = 0$, 0.14, 0.17 and 0.41 for cooling and heating runs (10 K min^{-1}).

Table 5. DSC data for the mixed DMACAB crystals with various Bi contents (x). T_c, ΔT, ΔH and ΔS stand for the transition temperature (taken during cooling), the temperature hysteresis of the transition extrapolated to zero scanning rate, the enthalpy and the entropy of the phase transition, respectively.

x	T_{c1} (K) on cooling	ΔT (K)	ΔH (kJ mol^{-1})	ΔS (J mol^{-1} K^{-1})	T_{c2} (K) on cooling	ΔT (K)	ΔH (kJ mol^{-1})	ΔS (J mol^{-1} K^{-1})
0	241	—	—	—	—	—	—	—
0.05	239	—	—	—	—	—	—	—
0.09	232	—	—	—	—	—	—	—
0.14	202	18.1	—	—	—	—	—	—
0.17	262	5.1	0.83	3.17	193	34.7	2.07	10.77
0.30	261	3.0	0.61	2.34	185	30.6	2.71	14.67
0.36	259	2.5	0.79	3.07	176	40.6	2.71	15.39
0.41	250	3.7	0.76	3.05	156	50.0	2.40	15.41

temperature phase transition is for all of these crystals accompanied by a larger enthalpy and a larger temperature hysteresis in comparison to those of the high-temperature one. Both phase transitions are shifted towards lower temperature with increase of the Bi content. This effect is stronger for the low-temperature phase transition.

Figure 6 shows the results on the linear thermal expansion, $\Delta L/L_0$, measured along the a-axis (monoclinic system) for DMACAB samples with $x = 0$, 0.05, 0.09, 0.14 and along

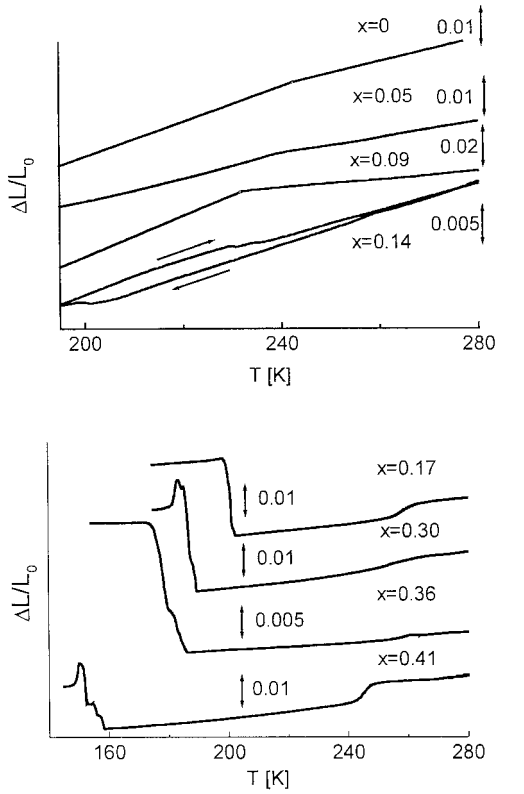

Figure 6. Temperature dependences of the linear thermal expansion for samples with (top) $x = 0$, 0.05, 0.09, 0.14 along the a-axis (monoclinic system) and (bottom) $x = 0.17$, 0.30, 0.36 and 0.41 along the c-axis (orthorhombic system) during cooling runs.

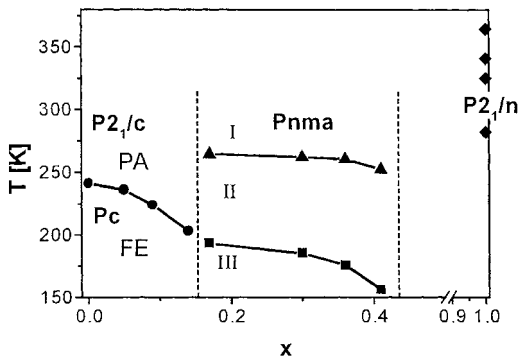

Figure 7. The phase diagram of the mixed DMACAB crystals.

the c-axis (orthorhombic system) for samples with $x = 0.17$, 0.30, 0.36 and 0.41. We can state that these results conform well with those obtained from the DSC measurements. For mixed DMACAB crystals with $0 \leqslant x \leqslant 0.14$ the changes in thermal dilatation are typical of a second-order phase transition, i.e. only the change in the temperature coefficient of the thermal dilatation is observed close to the phase transition. On cooling, for crystals with small

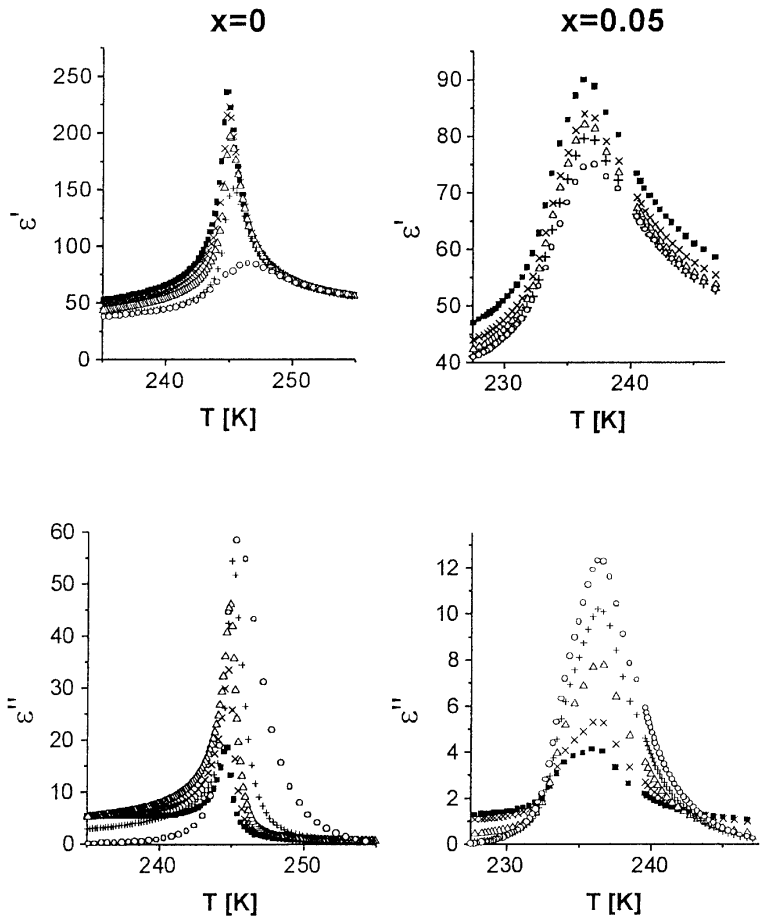

Figure 8. Temperature dependences of ε' (top) and of ε'' (bottom) for the DMACAB crystals with the Bi content $x = 0$, 0.05, 0.09, 0.14 along the c-axis.

Bi content ($0 \leqslant x \leqslant 0.09$), an increase in the slope of $\Delta L/L_0$ is found. The thermal expansion of the crystal with $x = 0.14$ reveals unexpectedly a small abrupt contraction typical of a first-order phase transition. For this crystal we also observe the presence of temperature hysteresis of the dilatometric anomaly.

Two anomalies in the thermal dilation corresponding to the first-order phase transitions are found for DMACAB crystals with $0.17 \leqslant x \leqslant 0.41$ (see the lower part of figure 6). This is in agreement with the results of calorimetric measurements. At the high-temperature phase transition, subtle stepwise changes of $\Delta L/L_0$ are revealed. For the low-temperature phase transition a significantly larger jump of $\Delta L/L_0$ is found. Both dilatometric anomalies are present only on cooling, since the effects cannot be reversed well. This is associated with breaking of the crystal at T_{c2}.

The phase diagram showing the situation in the mixed DMACAB crystals established on the basis of DSC and dilatometric results is presented in figure 7. The points on the right-hand side of the diagram (at $x = 1.0$) clearly reveal the completely different sequence of the structural phase transitions found for the pure bismuth analogue, namely $[(CH_3)_2NH_2]_3Bi_2Cl_9$ [20].

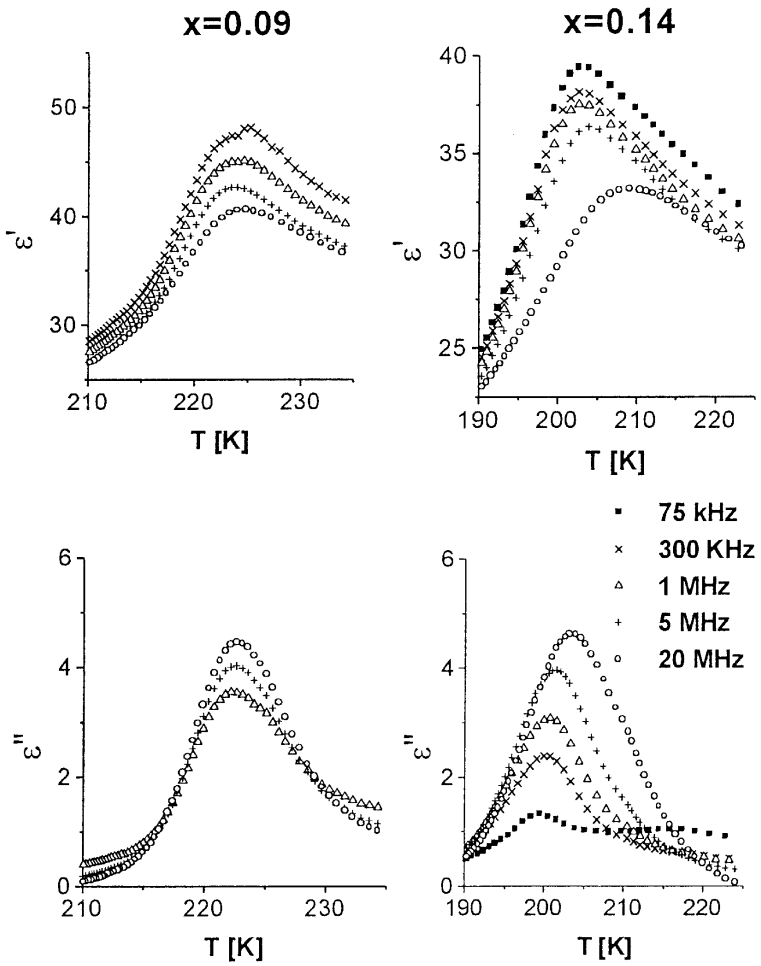

Figure 8. (Continued)

3.3. Dielectric relaxation studies

We performed measurements of the complex electric permittivity, ε^*, as a function of temperature and frequency for the pure antimony analogue, DMACA, and for the mixed crystals DMACAB ($x = 0.05$, 0.09, 0.14, 0.17, 0.30, 0.36 and 0.41). The purpose of these measurements was to determine the nature of the phase transitions and to establish the parameters of the existing dielectric relaxation processes.

The first group of dielectric results presented concerns the mixed crystals for Bi content in the range $0 < x < 0.14$, which preserve the polar properties. The $0.14 < x < 0.17$ composition range appears to be a 'critical' one for the disappearance of polar properties of the mixed crystals. Figure 8 shows the temperature dependences of the real and imaginary parts of the complex electric permittivity, $\varepsilon_c^* = \varepsilon_c' - \mathrm{i}\varepsilon_c''$, for samples with $0 \leqslant x \leqslant 0.14$ over the frequency range from 75 kHz to 20 MHz. For pure DMACA we observe a typical lambda-shaped curve for the ε_c' versus T dependence. It is clearly seen that with increase of the Bi content the shape of the dielectric response is spread over a broader temperature range and

the ε'-value at the maximum diminishes. The dielectric anomaly connected with the PE-to-FE transition shifts towards lower temperatures with increase of the Bi concentration, similarly to what is observed in the calorimetric and dilatometric measurements.

Figure 9 shows the temperature dependence of ε'_c (at 20 MHz) for mixed DMACAB crystals over the composition range $0.17 \leqslant x \leqslant 0.41$. For all systems investigated, two anomalies have been observed in ε' versus T runs. In the ordered low-temperature phase the ε'-value ($\approx$10) is comparable for all crystals considered. The low-temperature phase transitions are characterized by a stepwise change in ε'. The dielectric increment ($\Delta\varepsilon$) increases with diminishing bismuth content. In the intermediate-temperature phase, increase of ε' with increase of the temperature is observed. The high-temperature phase transition is also accompanied by a rapid jump in the ε'-value, but the dielectric increment is substantially lower. Further heating causes insignificant decrease of ε'. Both the low-temperature and the high-temperature phase transitions shift towards lower temperature with increase of the bismuth content.

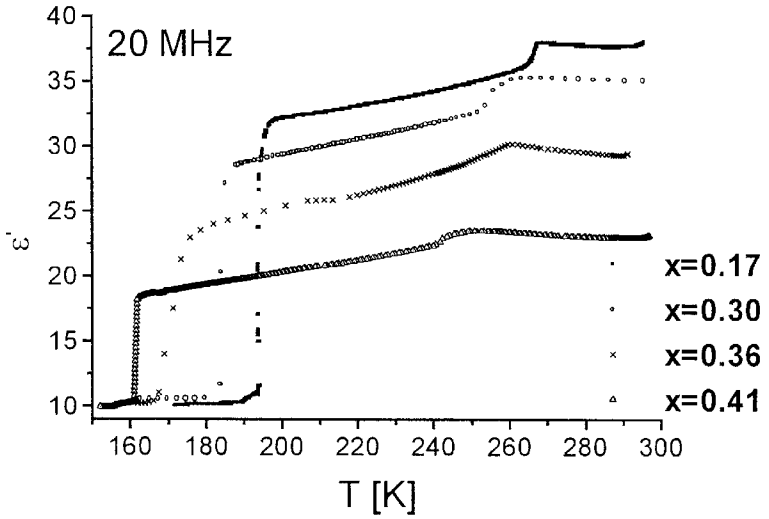

Figure 9. The temperature dependence of ε' for the DMACAB crystals with the Bi content $x = 0.17, 0.30, 0.36, 0.41$ along the c-axis.

The results obtained in the low-frequency region for the mixed DMACAB crystals ($x = 0.14$) suggest the existence of a relaxation process at higher frequencies. Therefore, studies of the temperature and frequency dependence of the electric permittivity in the high-frequency region (30–900 MHz) were undertaken. The temperature dependences of ε' and ε'' are shown in figure 10. It has been found that the dielectric response in these mixed crystals is well described by the Cole–Cole relation [21]:

$$\varepsilon^* = \varepsilon_\infty + \frac{\varepsilon_0 - \varepsilon_\infty}{1 + (\mathrm{i}\omega\tau)^{1-\alpha}} \tag{1}$$

where ε_0 and ε_∞ are the low- and high-frequency limits of the electric permittivity, respectively, ω is the angular frequency, τ is the mean relaxation time and α is the distribution of the relaxation times parameter.

We have fitted the experimental Cole–Cole plots at several temperatures with equation (1) and determined the fitting parameters ε_0, ε_∞, α and τ. The parameters of the low-frequency relaxation process (relaxator 1) are collected in table 6. The almost temperature-independent

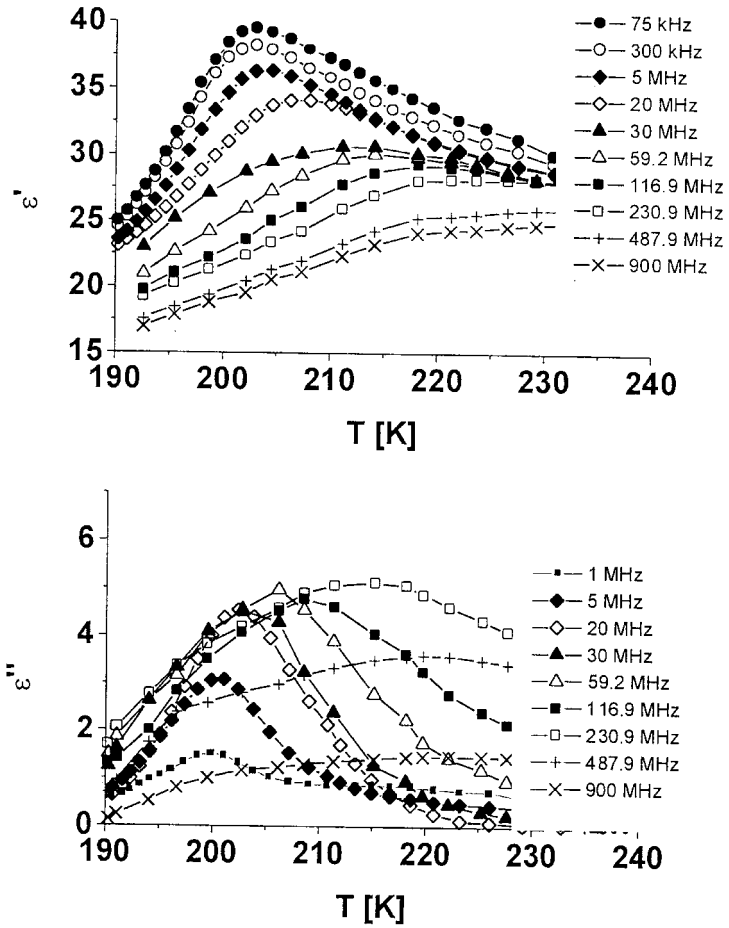

Figure 10. Temperature dependences of ε_c' (top) and of ε_c'' (bottom) for the DMACAB crystals with the Bi content $x = 0.14$ in the frequency range between 20 MHz and 900 MHz.

value of ε_∞ of about 21 is comparable to that found for the pure antimony analogue DMACA ($\varepsilon_\infty \approx 20$). An important increase in the mean relaxation time τ on cooling (about one order of magnitude over an interval of 20 K) shows a substantial slowing down of the relaxation process. The simultaneous increase in the distribution parameter α up to a value of about 0.36 at T_c shows that the dielectric spectrum becomes extremely diffuse.

In the case of the ferroelectric systems, the microscopic relaxation time, τ_0, is related to the macroscopic one, τ, according to

$$\tau_0 = \frac{\varepsilon_\infty}{\varepsilon_0 - \varepsilon_\infty}\tau. \tag{2}$$

Since the macroscopic relaxation time for the relaxation process exhibits critical slowing down, the energy barrier E_a was estimated from the Arrhenius relation for the microscopic relaxation time:

$$\tau_0 = C \exp\left(\frac{E_a}{kT}\right). \tag{3}$$

Cole–Cole diagrams at selected temperatures (between 205 and 220 K) above the phase transition temperature $T_c = 202$ K for DMACAB ($x = 0.14$) crystals are presented in

Table 6. Fit parameters for the low-frequency relaxation process in DMACAB ($x = 0.14$).

T (K)	ε_0	ε_∞	α	τ (10^{-10} s)
202	38.3	20.0	0.36	42
205	37.9	21.1	0.26	28
208	35.9	20.9	0.18	24
210	35.8	21.3	0.19	16
213	33.5	20.6	0.09	13
217	32.0	21.2	0.07	8.3
220	31.4	20.8	0.07	5.9
224	29.8	20.3	0.06	3.8

figure 11. These results indicate the existence of at least two different relaxation regions, low- and high-frequency ones. Far from T_c the diagrams for the low-frequency relaxation process are characterized by a small distribution of relaxation times. On approaching the phase transition point this distribution becomes greater. The activation energy estimated for this process (see figure 12) is equal to 0.27 eV and is rather high for such crystals [13, 22].

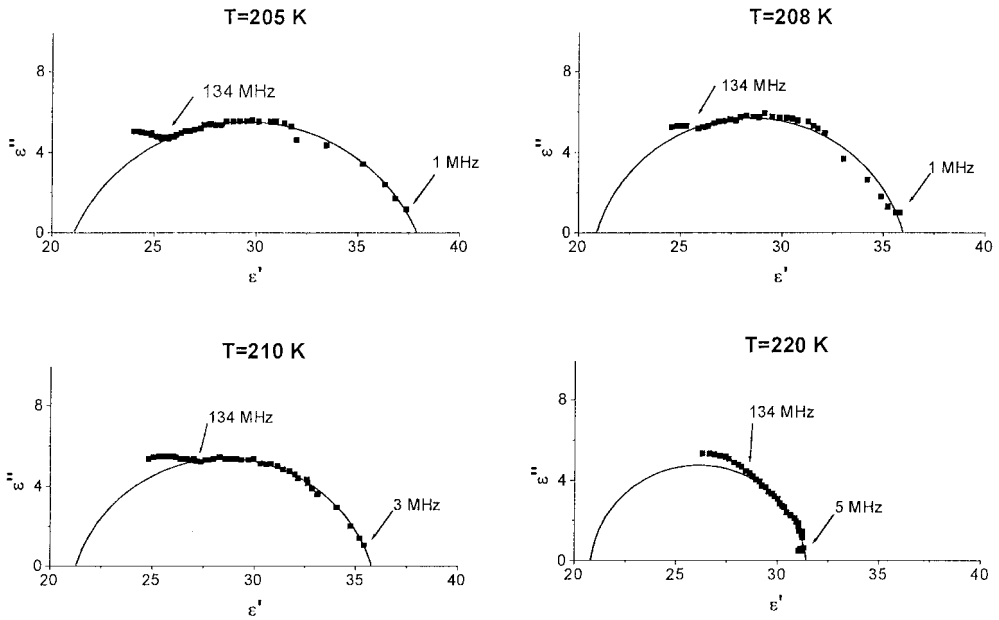

Figure 11. Cole–Cole diagrams for the DMACAB crystals with the Bi content $x = 0.14$ in the paraelectric phase.

The value of the relaxation time of the high-frequency relaxation process, τ_2, differs only by one order of magnitude from that obtained for the low-frequency relaxation, τ_1. Such a small difference between these two relaxation times is the main reason for the difficulty in estimating the values of the parameters for this process with sufficient accuracy. It should be noted, however, that the value of ε_∞ estimated for the low-frequency process is relatively large. It is comparable with that found for pure DMACA, for which an additional high-frequency process was also postulated. The presence of the onset of the high-frequency relaxation process (see the high-frequency side of the Cole–Cole diagrams in figure 11) may suggest that in the

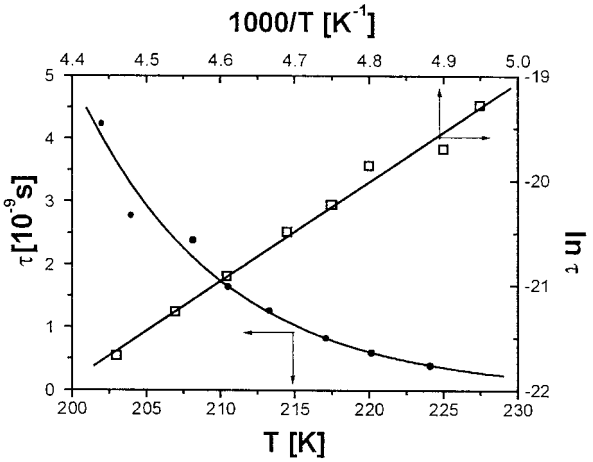

Figure 12. The temperature dependence of the macroscopic relaxation time τ (left and bottom) and $\ln(\tau)$ versus T^{-1} (right and top) around 202 K for the DMACAB crystals with the Bi content $x = 0.14$.

mixed DMACAB crystals the anticipated high-frequency relaxator relaxes more slowly than in the pure DMACA. It is impossible, however, to estimate the activation energy for this relaxator since the relaxation times obtained are burdened by a relatively large error.

In order to investigate the dynamics of the dipolar dimethylammonium groups in the non-ferroelectric mixed crystals ($x \geqslant 0.17$), dielectric relaxation studies were performed over a wide frequency range (75 kHz–900 MHz). Figure 13 presents the temperature dependences of ε_c' and ε_c'' in the range 20–900 MHz for the sample with $x = 0.17$. Two well shaped anomalies are found around the phase transition points at $T_{c1} = 262$ K and $T_{c2} = 193$ K. The jump in ε_c' observed at the low-temperature phase transition is several times bigger than that observed at the high-temperature one. At the high-temperature phase transition some kind of dielectric relaxation is, remarkably, disclosed (see the inset in figure 13). These preliminary dielectric dispersion studies on DMACAB ($x = 0.17$) indicate the presence of a low-frequency relaxation process around the I $\rightarrow$ II phase transition and an onset of the high-frequency relaxation process which is closely connected with the II $\rightarrow$ III phase transition. The low-frequency relaxation process at the I $\rightarrow$ II transition is well described by the contributions of two relaxators, which are quite well separated. The detailed analysis of the dielectric data in the high-frequency region for DMACAB ($x = 0.17$) will be the subject of a separate paper.

3.4. Spontaneous polarization measurements

The dielectric response of the mixed DMACAB ($x < 0.14$) salts is still typical of ferroelectric crystals. Spontaneous polarization (P_s) measurements were undertaken to analyse the influence of the bismuth content on polar properties. The observed values of P_s in the mixed DMACAB crystals were obtained after preliminary poling by an external field of the order of ± 1000 V cm^{-1}. The temperature dependence of the spontaneous polarization P_s for the pure DMACA crystal and that for DMACAB ($x = 0.09$ and 0.14) are displayed in figure 14. The temperature characteristic of P_s for the pure DMACA is typical of a second-order phase transition and P_s for this crystal reaches a value of 8.5×10^{-3} C m^{-2}. The partial replacement of the antimony by bismuth atoms in the lattice of DMACA causes a distinct reduction of the saturated P_s-value (to 6×10^{-4} C m^{-2} and 4×10^{-4} C m^{-2} for DMACAB with $x = 0.09$

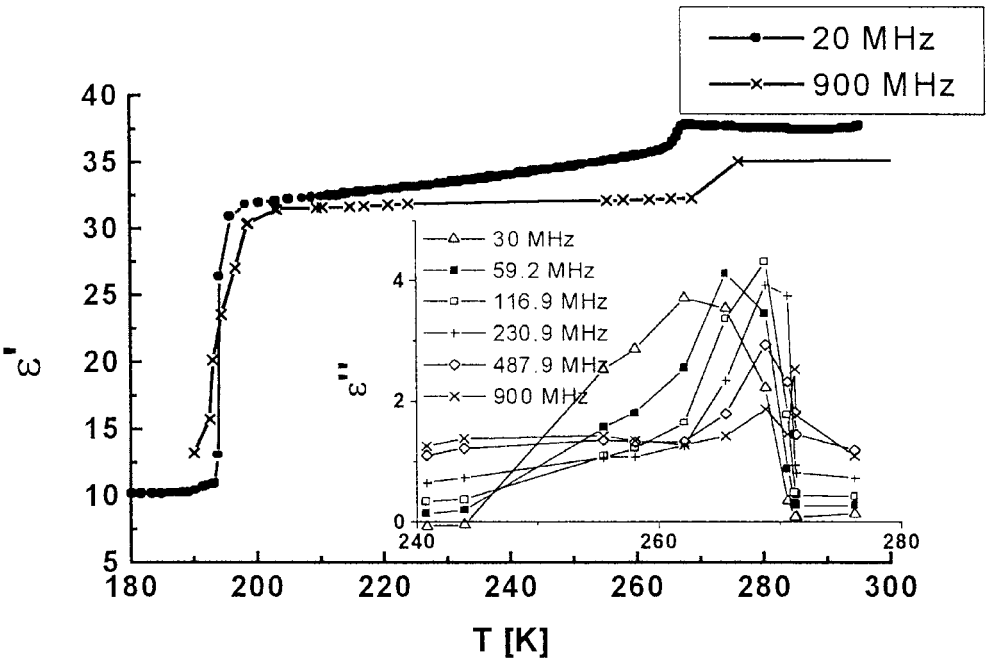

Figure 13. Temperature dependences of ε_c' (main figure) and of ε_c'' (inset) for the DMACAB crystals with the Bi content $x = 0.17$ in the frequency range between 75 kHz and 900 MHz.

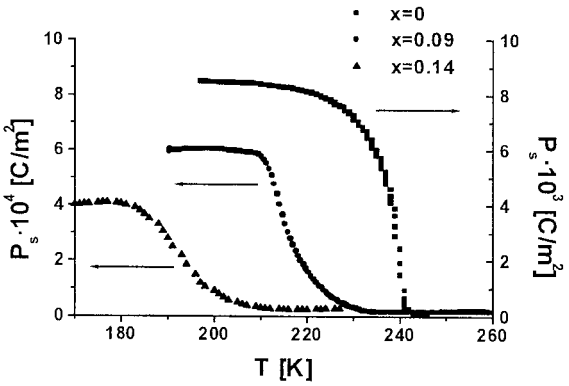

Figure 14. Temperature dependences of the spontaneous polarization P_s for the pure DMACA crystal and for DMACAB ($x = 0.09$ and 0.14).

and 0.14, respectively). The mixed crystals exhibit additionally a distinct tail on the P_s versus T curve above the FE $\rightarrow$ PE phase transition temperature. A similar tendency in the reduction of the P_s-value was observed for the $(CH_3NH_3)_5Bi_{2(1-x)}Sb_{2x}Cl_{11}$ [23] and $[N(CH_3)_3H]_3Sb_{2(1-x)}Bi_{2x}Cl_9$ mixed crystals [24]. In these crystals also a drastic lowering of the P_s-value for the mixed systems in comparison to that in the pure salts is observed.

It is interesting to note that the variation of P_s with increase of the temperature for $x = 0.09$ shows a tendency to go to zero just above 225 K in a manner reminiscent of the second-order phase transition. This effect is probably prevented by the presence of field-alignable dipolar

clusters; it is even more enhanced for $x = 0.14$. In the case of crystals with $x = 0.14$ the inflection point in P_s versus T close to the phase transition point may indicate a change in the nature of the domain alignment. Dipolar clusters existing above 202 K undergo relaxational freezing, which is clearly visible in $x = 0.14$ samples (see figure 14). This type of behaviour is typical of ferroelectric relaxors (glass systems).

4. Discussion

4.1. Non-ferroelectric systems ($0.17 \leqslant x \leqslant 0.41$*)*

The dielectric results presented for the non-ferroelectric systems allow us to note two different aspects related to the effect of Sb $\rightarrow$ Bi replacement. The first is related to a change of polarizability of the system connected with the modification of the anionic sublattice. The second is related to the change in the dynamics of the cationic sublattice, which is reflected in the magnitude of the macroscopic relaxation time.

The dielectric anomaly corresponding to the high-temperature phase transition smears with increase of the Bi content, whereas the low-temperature anomaly does not change its character, i.e. its dielectric response is characteristic of systems with the 'rotator' phase. It is clearly seen that after freezing of the rotational motion of the dimethylammonium cations, ε'_c reaches a value of about 10 units, which is undoubtedly comparable to the optical value, ε_∞. The dielectric strength ($\Delta\varepsilon$) encountered in mixed alkylammonium halogenoantimonate(III)–bismuthate(III) salts is very sensitive to the Sb/Bi ratio. In the title crystal we observe an almost twofold reduction in the dielectric increment value when the bismuth content changes from $x = 0.17$ to $x = 0.41$ (see figure 9). This effect has already been observed for the other mixed systems, e.g. for $(CH_3NH_3)_3Sb_{2(1-x)}Bi_{2x}Cl_9$ [25]. It is interesting that for both the dimethylammonium and methylammonium analogues [25] characterized by one-dimensional polyanionic structure (type a) over their 'rotator' phase (for DMACAB above T_{c2}), the dielectric strength decreases with increase of the bismuth content.

On the other hand the larger concentration of the bismuth should enhance the polarizability of the systems studied due to the larger polarizability of the Bi atoms in comparison to that of the Sb ones. This implies that the decisive role, taking into account the contribution to the dielectric strength, is played by the dipole–dipole interactions of the methylammonium or dimethylammonium groups rather than by the enhanced polarizability of Bi atoms. The increase of the bismuth concentration seems to reduce the dipole–dipole interactions of the mixed crystals.

The characteristic feature of the crystals discussed above is relatively fast reorientation of dipolar cations, either methylammonium or dimethylammonium ones in the 'rotator' phase. In the case of pure methylammonium crystals $(CH_3NH_3)_3Sb_2Cl_9$ and mixed analogues [25], the relaxation frequency indicates that the macroscopic relaxation time is shorter than 10^{-9}–10^{-10} s, whereas for the dimethylammonium derivatives (for $x > 0.17$) the relaxation processes take as little as about 10^{-8} s. This difference is explained by an increase of the moment of inertia of the rotating dipoles and/or by an increase of the cation dimension.

4.2. Ferroelectric systems ($0 \leqslant x \leqslant 0.14$*)*

The temperature of the PE $\rightarrow$ FE phase transition is the parameter most sensitive to the replacement of antimony by bismuth in the ferroelectric mixed $[(CH_3)_2NH_2]_3Sb_{2(1-x)}Bi_{2x}Cl_9$ crystals ($0 < x < 0.14$). An increase in the Bi concentration lowers the PE-to-FE phase transition temperature ($dT_c/dx = -143$ K). This is accompanied by a strong reduction of

both the electric permittivity at T_c and the P_s-value. Such behaviour is typical of the $R_3M_2X_9$ systems. Similar effects were found in the mixed trimethylammonium analogues [24].

On the other hand, the changes in the dynamic dielectric properties of the mixed ferroelectric dimethylammonium crystals ($0 < x < 0.14$) are rather weak. Far from the phase transition point the dynamic properties of DMACA and of the $x = 0.14$ crystals are comparable. The differences become more pronounced approaching the phase transition point. In the close vicinity of T_c the macroscopic relaxation time of DMACA is twice as large as in the DMACAB ($x = 0.14$) crystal (see table 7). Such behaviour is anticipated, since the slowing down is more significant (critical) for the lower-defect-content ferroelectric systems. It should also be noted that the reorientation of single dipoles in the pure dimethylammonium analogue (DMACA) is characterized by distinctly lower activation energy (0.16 eV [13]) in comparison to that found for the $x = 0.14$ crystal (0.27 eV). The most probable reason for this difference is the steric effect connected with the deformation of the twelve-membered cavities occupied by the N(2) cations.

Table 7. Dielectric parameters for the ferroelectric relaxation for the dimethylammonium crystals. (τ_1: macroscopic relaxation time for the low-frequency relaxation at T_c; E_{a1}: corresponding activation energy estimated for the microscopic relaxation time; τ_2: relaxation time for the high-frequency relaxation; E_{a2}: corresponding activation energy.)

	DMACA ($T_c = 242$ K)	DMACAB ($x = 0.14$, $T_c = 202$ K)	DMABA ($T_c = 164$ K)
$\Delta\varepsilon_{max,1}(T_c)$	~ 230	~ 18	~ 40
τ_1 (s)	9×10^{-9}	4.2×10^{-9}	10^{-7}
E_{a1} (eV)	0.16	0.27	0.23
τ_2 (s)	$< 10^{-11}$	$< 10^{-10}$	$\sim 10^{-11}$
E_{a2} (eV)	?	?	0.04
Reference	[13]	This work	[13, 18]

Since DMABA, DMACA and its mixed analogue with $x = 0.14$ are isomorphous ($P2_1/c$) at room temperature, one may expect closely related dynamical properties of the cationic sublattice in the paraelectric phase. The dynamic dielectric behaviours of these three crystals around the PE $\rightarrow$ FE transitions are determined by the presence of two independent dielectric relaxators strictly connected with two types of crystallographically non-equivalent DMA cations. The low-frequency ferroelectric relaxator exhibits a critical slowing down close to T_c, whereas the high-frequency one is only thermally activated. A comparison of the parameters characterizing the dielectric relaxators is given in table 7.

A similar dynamic situation is observed in the other ferroelectric chloroantimonates(III) having two-dimensional anionic structure, namely $[(CH_3)_3NH]_3Sb_2Cl_9$ and its mixed system $[(CH_3)_3NH]_3Sb_{2(1-x)}Bi_{2x}Cl_9$ [24]. Comparison of the influence of the replacement of the antimony atoms by bismuth ones in the dimethylammonium and trimethylammonium analogues mentioned above leads to the following conclusion: an increase of bismuth concentration in both systems leads to a progressive deformation of the ideal two-dimensional anionic structure. In the case of the trimethylammonium derivatives for $x > 0.33$ and for the dimethylammonium one for $x > 0.14$, the destruction of the $M_2X_9^{3-}$ layer structure follows. The isolated bioctahedral units and one-dimensional double chains appear for the trimethylammonium and dimethylammonium analogues, respectively. This seems to be the direct reason for the disappearance of the polar properties. It clearly confirms that the presence of the two-dimensional layers of the anionic sublattice is a necessary condition for the existence of ferroelectricity in the $R_3M_2X_9$-type compounds.

Taking into account the temperature characteristics of P_s for various contents of Bi in the mixed DMACAB systems and those of $(CH_3NH_3)_5Bi_2Cl_{11(1-x)}Br_{11x}$ [26], one should underline the important differences. For the former crystals the value of P_s is strongly reduced with increase of the bismuth content. It is interesting to note that in the case of the ferroelectric mixed salts of $R_5Bi_2X_{11}$ stoichiometry, the P_s-value changes continuously, being in the range characteristic for the pure analogues: $(CH_3NH_3)_5Bi_2Cl_{11}$ and $(CH_3NH_3)_5Bi_2Br_{11}$ ($P_s = 1.0$ and 1.6×10^{-2} C m^{-2}, respectively). Such a temperature characteristic of P_s for these salts may be explained in the following way. The pure methylammonium analogues are isomorphous and exhibit ferroelectric properties. For the intermediate composition (Cl $\rightarrow$ Br) we should not expect significant deformation of the anionic sublattice (isolated $Bi_2X_{11}^{5-}$ units). This explains the continuous changes in the spontaneous polarization value. In the case of crystals, for which the ferroelectricity is determined by the presence of polyanionic layers, the situation is different. The Bi substitution in DMACA analogues may be explained in terms of the change of impurities (defects) in the crystal lattice. It causes progressive deformation of the anionic structure, which is reflected in a diminishing of the P_s-value. At a critical concentration of impurities ($0.14 < x < 0.17$) the cracking of the layers and disappearance of the polar properties of the crystal take place.

The most important conclusion from the present studies is that the preserving of the polar properties in the mixed crystals requires maintaining of the anionic layer structure (type b). In order to improve the dielectric characteristics of the salts studied, incorporation in the crystal lattice of cationic units with large dipolar polarizability, without any breaking of the two-dimensional polyanionic sublattice, is desirable.

5. Conclusions

To summarize, we have carried out a detailed study of the variation of the complex electric permittivity, $\varepsilon^*(\omega, T)$, with temperature at various frequencies from 75 kHz to 900 MHz for the $[NH_2(CH_3)_2]Sb_{2(1-x)}Bi_{2x}Cl_9$ mixed crystals ($x = 0.05, 0.09, 0.14, 0.17, 0.30, 0.38, 0.41$). To confirm the polar properties we have also performed polarization measurements as a function of temperature using the pyroelectric technique (for $x = 0.0$, 0.09 and 0.14).

The DSC and dilatometric measurements allowed us to establish the phase situation for these mixed crystals.

The salts with $0 \leqslant x \leqslant 0.14$ crystallize in the monoclinic $P2_1/c$ space group and undergo continuous PE $\rightarrow$ FE transition, whereas those with $0.17 \leqslant x \leqslant 0.41$ (orthorhombic $Pnma$ space group, phase I) reveal two non-continuous structural phase transitions below room temperature without showing any polar phases.

Our results conclusively establish that the ferroelectric phase in DMACAB is stable for $x \leqslant 0.14$. The characteristic feature of the dynamic dielectric response in the paraelectric phase for the ferroelectric system is the presence of two relaxation modes: a low-frequency one exhibiting a critical slowing down ($\tau_{1\,(\mathrm{at}\,T_c)} \approx 10^{-8}$ s) and a high-frequency one, probably only thermally activated.

In the case of non-ferroelectric systems, for $x \geqslant 0.17$, the high-temperature, 'rotator-like' phase reveals relaxation processes connected with the dynamics of the disordered dimethylammonium cations.

The disappearance of ferroelectric properties is related to the essential changes in the crystal structure of the mixed compounds studied. The characteristic feature of the ferroelectric DMACAB mixed crystals ($0.0 \leqslant x \leqslant 0.14$) is the presence of polyanionic $(M_2Cl_9^{3-})_n$ layers, whereas non-ferroelectric ones are characterized by a different anionic sublattice composed of polyanionic one-dimensional double chains of polyhedra.

Acknowledgments

This work was supported by the Polish State Committee for Scientific Research (project register 7 T09A 070 21).

References

[1] Jakubas R and Sobczyk L 1990 *Phase Transitions* **20** 163
[2] Sobczyk L, Jakubas R and Zaleski J 1997 *Polish J. Chem.* **71** 265
[3] Iwata M and Ishibashi Y 1992 *Ferroelectrics* **135** 283
[4] Iwata M, Miyashita A, Orihara H, Ishibashi Y, Kuok M H, Rang Z L and Ng S C 1999 *Ferroelectrics* **229** 233
[5] Carpentier P, Zielinski P and Lefebvre J 1997 *Z. Phys.* B **102** 403
[6] Jóźków J, Bator G, Jakubas R and Pietraszko A 2001 *J. Chem. Phys.* **114** 7239
[7] Jakubas R, Czapla Z, Galewski Z, Sobczyk L, Żogał O J and Lis T 1986 *Phys. Status Solidi* a **93** 449
[8] Kallel A and Bats J W 1985 *Acta Crystallogr.* C **41** 1022
[9] Chabot B and Parthe E 1978 *Acta Crystallogr.* B **34** 645
[10] Aurivilius B and Stalhandske C 1978 *Acta Chem. Scand.* A **32** 715
[11] Jakubas R 1986 *Solid State Commun.* **60** 389
[12] Zaleski J and Pietraszko A 1996 *Acta Crystallogr.* B **52** 287
[13] Bator G and Jakubas R 1995 *Phys. Status Solidi* a **147** 591
[14] Bator G, Jakubas R, Lefebvre J and Guinet Y 1998 *Vib. Spectrosc.* **18** 203
[15] Miniewicz A, Lefebvre J and Jakubas R 1991 *J. Raman Spectrosc.* **22** 435
[16] Sheldrick G M 1997 *SHELXL97 Program for the Refinement of Crystal Structures*
[17] Gdaniec M, Kosturkiewicz Z, Jakubas R and Sobczyk L 1988 *Ferroelectrics* **77** 31
[18] Zaleski J, Pawlaczyk Cz, Jakubas R and Unruh H-G 2000 *J. Phys.: Condens. Matter* **12** 7509
[19] Jakubas R, Tomaszewski P and Sobczyk L 1989 *Phys. Status Solidi* a **111** K27
[20] Jakubas R *et al* 2001 in preparation
[21] Cole K S and Cole R H 1941 *J. Chem. Phys.* **9** 341
[22] Sobiestianskas R, Czapla Z and Grigas J 1992 *Phys. Status Solidi* a **130** K69
[23] Bator G, Mróz J and Jakubas R 1997 *Physica* B **240** 362
[24] Bator G, Jakubas R, Zaleski J and Mróz J 2000 *J. Appl. Phys.* **88** 1015
[25] Jakubas R, Bator G, Zaleski J, Pietraszko A and Decressain R 1996 *J. Phys.: Condens. Matter* **8** 367
[26] Mróz J and Jakubas R 1996 *Ferroelectrics* **189** 173